Konya Mühendislik Bilimleri Dergisi, c. 10, s. 3, 548-562, 2022
Konya Journal of Engineering Sciences, v. 10, n. 3, 548-562, 2022
ISSN: 2667-8055 (Electronic)
DOI: 10.36306/konjes.1107094

NUMERICAL EXAMINATION OF A SOLAR CHIMNEY POWER PLANT DESIGNED FOR THE ISKENDERUN REGION

[1]Mustafa ÖNAL, [2]Ali KOÇ, [3]Özkan KÖSE, [4]Yıldız KOÇ, [5]Hüseyin YAĞLI

[1, 2, 3, 4] *Department of Mechanical Engineering, Faculty of Engineering and Natural Sciences, İskenderun Technical University, Iskenderun, Hatay, TURKIYE*
[5] *Mechanical Engineering Department, Engineering Faculty, Gaziantep University, Gaziantep, TURKIYE*
[1]mustafa.onal@iste.edu.tr, [2]ali.koc@iste.edu.tr, [3]ozkan.kose@iste.edu.tr, [4]yildiz.koc@iste.edu.tr, [5]yagli@gantep.edu.tr

Geliş/Received: 21.04.2022; Kabul/Accepted in Revised Form: 14.06.2022

ABSTRACT: Today, energy is accepted as the most indicator of economic development. However, the use of fossil fuels as energy sources is caused the depletion of the ozone layer, global warming and climate change. Therefore, using renewable energy systems called sustainable energy is a remarkable step in terms of both minimizing fossil fuel consumption and the effects of the environment on human health. In this study, solar chimneys, one of the solar-assisted electricity generation systems among renewable energy sources, are analyzed. A solar chimney power plant (SCPP) has been designed by considering the environmental conditions of the Iskenderun region in Hatay province. The facility consists of collector, chimney, turbine and generator. Sun rays entering the solar chimney from the transparent collector heat the air. The heated air leaves the solar chimney with the effect of the pressure difference. The turbine is placed in the chimney section where the air velocity is high. The mechanical power obtained from the turbine is converted into electrical energy through the generator. The energy source of the system is the sun, and the working fluid of the system is air. In the calculations, the average irradiance value of the Iskenderun region was used and optimization of the designed SCPP was made using these values. The optimization of the SCPP designed for the Iskenderun region is performed using numerical analysis programs.

Keywords: Solar chimney, Renewable energy, Solar energy, CFD

İskenderun Bölgesi İçin Tasarlanan Güneş Baca Santrali Sayısal İncelemesi

ÖZ: Günümüzde enerji, ekonomik gelişmişliğin en önemli göstergesi olarak kabul edilmektedir. Ancak fosil yakıtların enerji kaynağı olarak kullanılması ozon tabakasının incelmesi, küresel ısınma ve iklim değişikliğine neden olmaktadır. Bu nedenle sürdürülebilir enerji olarak adlandırılan yenilenebilir enerji sistemlerinin kullanılması hem fosil yakıt tüketimini en aza indirmek hem de çevrenin insan sağlığına etkileri açısından dikkate değer bir adımdır. Bu çalışmada yenilenebilir enerji kaynaklarından güneş enerjisi destekli elektrik üretim sistemlerinden biri olan güneş bacaları incelenmiştir. Hatay ili İskenderun bölgesinin çevre koşulları dikkate alınarak güneş bacalı elektrik santrali (SCPP) projelendirilmiştir. Tesis kollektör, baca, türbin ve jeneratörden oluşmaktadır. Şeffaf kollektörden güneş bacasına giren güneş ışınları havayı ısıtmaktadır. Isınan hava, basınç farkının etkisiyle güneş bacasını terk etmektedir. Türbin, hava hızının yüksek olduğu baca bölümüne yerleştirilmektedir. Türbinden elde edilen mekanik güç, jeneratör vasıtasıyla elektrik enerjisine dönüştürülmektedir. Sistemin enerji kaynağı güneş, sistemin çalışma akışkanı ise havadır. Hesaplamalarda İskenderun bölgesinin ortalama ışınım değeri kullanılmış

ve bu değerler kullanılarak tasarlanan SCPP'nin optimizasyonu yapılmıştır. İskenderun bölgesi için tasarlanan SCPP'nin optimizasyonu sayısal analiz programları kullanılarak gerçekleştirilmektedir.

Anahtar Kelimeler: Güneş bacası, Yenilenebilir enerji, Güneş enerjisi, HAD

1. INTRODUCTION

Considering today's climatic conditions and the fluctuating epidemic process, energy constitutes the lifeblood of economies for developed or developing countries. In addition, the closure of countries and the disruption of supply processes, the increasing population density cause an increase in the burden on e-commerce, and therefore, the dependence on technology is constantly increasing. As a result of this, problems in energy supply and the inability to meet the demand are seriously on the agenda. Also, a bigger problem is the depletion of fossil fuels and the inability to fully improve energy sources that can replace them (Mert et al., 2020). For this reason, serious studies are being carried out on the variety of new systems suitable for non-traditional renewable energy sources such as solar, wind, hydroelectric and biomass (Karami et al., 2021; Tan et al., 2022; Nassar et al., 2021; Roy and Samanta, 2021; Koç et al., 2020). However, the most remarkable sustainable energy source among these energy sources is solar energy. Many serious studies continue on solar energy such as solar towers, parabolic trough systems, photovoltaic systems and combined systems. In this study, the solar chimney, which is one of the solar-assisted electricity generation systems, is discussed. SCPP is enabled carbon-free electricity generation leading to sustainable growth and development towards a green economy and a safer environment. It is also used for other applications such as air conditioning, desalination, electrical power generation and agri-food processing (Das and Chandramohan, 2020). SCPP has three basic components. These are the absorbing ground layer, the solar collector and the solar chimney. In addition, a turbine connected to the generator is required to convert the kinetic energy of the air into electrical energy (Das and Chandramohan, 2020). The theoretical concept of the solar chimney plant was first developed by Hanns Gunther at the beginning of the 19th century and the first plant was built in 1981 in Manzanares, Spain under the supervision of J. Schlaich, and the theoretical description of the solar chimney was provided by Haaf et al. (Haaf et al., 1983). Later, Schlaich et al. investigated the commercial and economic viability of a large-scale plant (up to 200 MW). Apart from these, there are many studies on solar chimneys. Sing et al. performed the CFD analysis of the hybrid PV and solar chimney, taking into account the solar radiation of 850 W/m^2, assuming zero inlet and outlet pressures. They used a solar chimney height of 3 meters and a collector radius of 1.5 meters. They made 4 different mesh improvements and reached the maximum number of 225820. Ultimately, the solar chimney power output of 2.258 W was obtained as the best result (Singh et al., 2020). Nasraoui et al. designed a conventional, parallel and counter-flow solar collector to increase the efficiency of the solar chimney. During the CFD analysis, a maximum of 300746 mesh was used and the solar chimney inlet and outlet pressures were accepted as zero. They also accepted the solar radiation as 880 W/m^2. As a result of their studies, they claimed that they increased the system efficiency up to 28% (Nasraoui et al., 2020). Kebabsa et al. investigated the solar chimney in two dimensions. A power of 0.34 W was obtained from the solar chimney with a height of 12.3 meters and a radius of 12.5 meters, and they claimed that the optimum collector inlet angle was 9.1 degrees (Kebabsa et al., 2020).

Considering all these studies, there is almost no study that used the working fluid that is accepted as compressible fluid. Besides, in most of the studies, the sun was not defined as well as the pressure difference that would occur due to the height difference between the chimney inlet and outlet was not defined. In this study, the working fluid was accepted as an ideal gas. The location of the İskenderun region, the date and time were selected and the sun was defined, the solar chimney outlet pressure was identified to the system by calculating the pressure drop depending on the height of the chimney.

2. SYSTEM DESCRIPTION

When designing SCPPs, the design should be made by considering many variables. Within the scope of this study, the parameters in Table 1 were accepted as constant.

Table 1. Beginning parameters for solar chimney

h (m)	R (m)	α (°)	β (°)	r (m)	a(m)	I (W/m²)
0.6	20	5	2	2.75	2	700

The main variables in the geometric design of the SCPP are; collector inlet height (h), collector radius (R), collector angle (α), divergent angle (β), chimney radius (r), radius of the curve between collector and chimney connection (a), solar radiation (I) and chimney height (H). The parameters in Table 1 were considered constant and optimization were performed for different chimney heights. The schematic outlook of the SCPP is shown in the Figure 1.

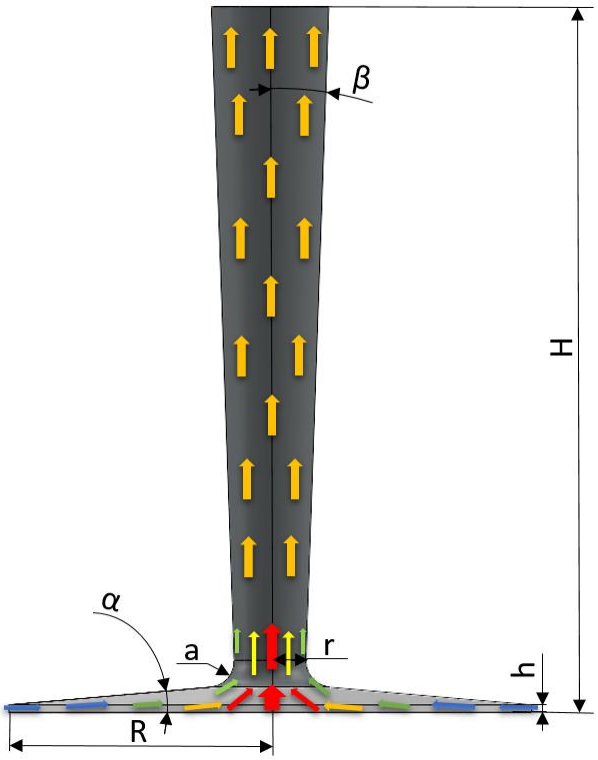

Figure 1. The schematic outlook of the SCPP

After the design parameters of the SCPP are identified in the numerical analysis program, it needs to be divided into many small parts. These parts are called meshes. As the number of mesh elements increases, the system is divided into smaller parts and more accurate results are obtained in the numerical analysis. The mesh structure of the solar chimney is shown in Figure 2.

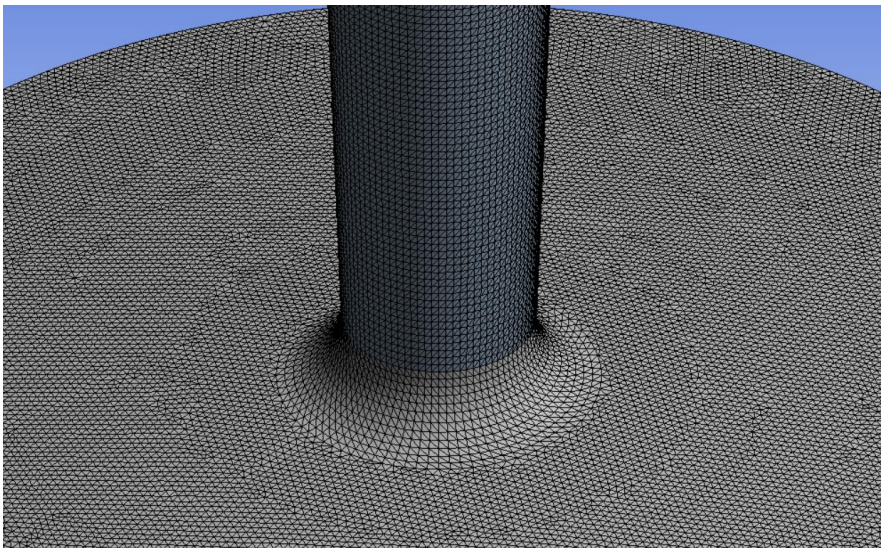

Figure 2. The mesh structure of the solar chimney

On the other hand, it is as important as the number of mesh elements in which regions the mesh is more frequent. The parameters such as velocity or temperature are shown rapidly changes in the regions near the surface. Therefore, the mesh should be tightened in the regions near the surface. In Figure 3, it is seen that the mesh applied on the SCPP becomes denser in a way that it consists of 3 layers in the regions near the chimney surface.

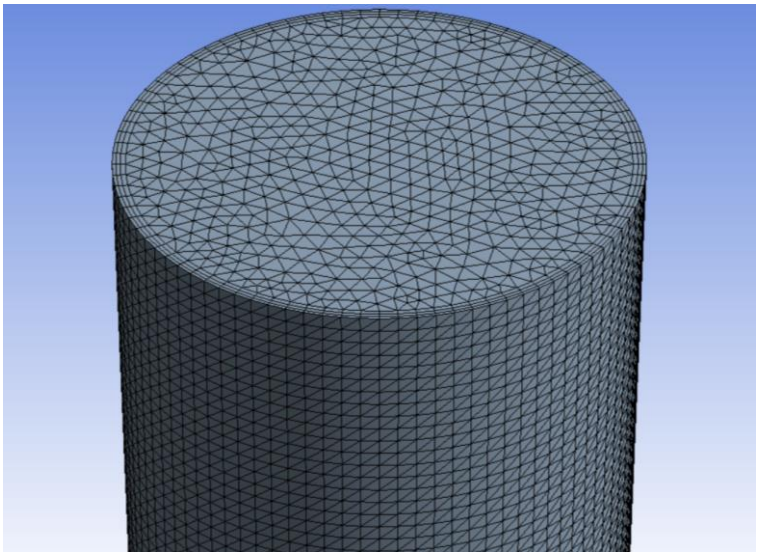

Figure 3. Mesh structure on the chimney outlet surface

This dense mesh structure consisting of 3 layers on the chimney surface continues throughout the collector. On the ground, the number of these dense layers has been increased to 4. The reason for this is that high temperature differences will occur at unit distances perpendicular to the ground, unlike the adiabatic chimney surface. The mesh structure in the air inlet area is given in the Figure 4.

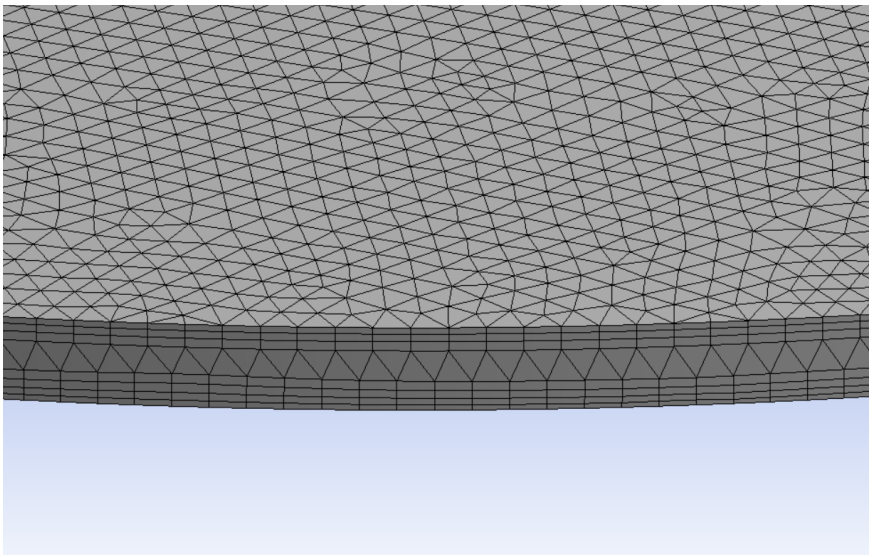

Figure 4. Mesh structure in the air inlet area

Considering the mesh properties above, for an SCPP with a chimney height of 50 m, the number of mesh elements and the number of nodes applied on the SCPP were carried out as 1384905 and 400394, respectively.

After the mesh structure was completed, the problem was defined in the numerical analysis program. While making these definitions, several different methods from the literature were used. The first of these differences is fluid selection. In many publications, the fluid has been chosen as an incompressible fluid, but in this study, the fluid has been accepted as an ideal gas. The second difference is that in many publications, the heat source was applied from the ground by determining an average heat flux or a constant temperature was determined for the ground. Another difference is related to the boundary conditions, the pressure of the air in the inlet and outlet regions of the system is defined as 101325 Pa in many publications. Table 2 shows the boundary conditions of the system.

Table 2. Boundary Conditions

Boundary Conditions	**Model features**
SCPP Inlet Pressure	$P_{in} = 101325$ Pa
Ambient Temperature	$T_0 = 300$ K
SCPP Output Pressure	$P_{out} = P_{in} - \rho . g . H$
Ground	Opaque
Collector	Transparent
Chimney	Opaque and insulated

3. MATHEMATICAL MODEL

The energy equations should be chosen considering the boundary conditions. In this study, Navier-Stokes and continuity equations are used to explain the flow in the x, y and z directions. The y-direction is opposite to the direction of the gravitational force (Cable, 2009).

The momentum in the x-direction;

$$\frac{\partial}{\partial t}(\rho u)+\frac{\partial}{\partial x}(\rho uu)+\frac{\partial}{\partial y}(\rho vu)+\frac{\partial}{\partial z}(\rho wu)=-\frac{\partial P}{\partial x}+\mu\left(\frac{\partial^2 u}{\partial x^2}+\frac{\partial^2 u}{\partial y^2}+\frac{\partial^2 u}{\partial z^2}\right) \quad (1)$$

The momentum in the y-direction;

$$\frac{\partial}{\partial t}(\rho v)+\frac{\partial}{\partial x}(\rho uv)+\frac{\partial}{\partial y}(\rho vv)+\frac{\partial}{\partial z}(\rho wv)=-\frac{\partial P}{\partial y}+(v+v_t)\left(\frac{\partial^2 v}{\partial x^2}+\frac{\partial^2 v}{\partial y^2}+\frac{\partial^2 v}{\partial z^2}\right) \quad (2)$$

The momentum in the z-direction;

$$\frac{\partial}{\partial t}(\rho w)+\frac{\partial}{\partial x}(\rho uw)+\frac{\partial}{\partial y}(\rho vw)+\frac{\partial}{\partial z}(\rho ww)=-\frac{\partial P}{\partial z}+(v+v_t)\left(\frac{\partial^2 w}{\partial x^2}+\frac{\partial^2 w}{\partial y^2}+\frac{\partial^2 w}{\partial z^2}\right) \quad (3)$$

Continuous flow equation;

$$\frac{\partial}{\partial x}(\rho u)+\frac{\partial}{\partial y}(\rho v)+\frac{\partial}{\partial z}(\rho w)=0 \quad (4)$$

Shih's Realizable model is lately the most remarkable model among the three k-ε variations for the SCPP. This model has two important differences from the standard k-ε model. It is used novel equality for turbulent viscosity, and the dissipation rate equation is obtained from the equality for transporting the mean square eddy fluctuation. The form of the eddy viscosity equations is dependent on feasibility constraints and the positivity of normal Reynolds stresses as well as the Schwarz inequality for turbulent shear stresses. The realizable k-ε model is more suitable and accurate than standard or RNG k-ε models in predicting flows like discrete flows and flows that have complex secondary flow characteristics (Shih et al., 1995). In this study, the realizable k-ε turbulence model was applied as a turbulence model. Transport equations for realizable k-ε turbulence model;

$$\frac{\partial}{\partial t}(\rho k)+\frac{\partial}{\partial x_j}\left(\rho k u_j\right)=\frac{\partial}{\partial x_j}\left[\left(\mu+\frac{\mu_t}{\sigma_\varepsilon}\right)\frac{\partial k}{\partial x_j}\right]+G_k+G_b-\rho\varepsilon-Y_m \quad (5)$$

$$\frac{\partial}{\partial t}(\rho \varepsilon)+\frac{\partial}{\partial x_j}\left(\rho k \varepsilon_j\right)=\frac{\partial}{\partial x_j}\left[\left(\mu+\frac{\mu_t}{\sigma_\varepsilon}\right)\frac{\partial \varepsilon}{\partial x_j}\right]+\rho C_1 S\varepsilon-\rho C_2\frac{\varepsilon^2}{k+\sqrt{\nu\varepsilon}}+C_{1\varepsilon}\frac{\varepsilon}{k}C_{3\varepsilon}G_b \quad (6)$$

While G_k represents the generation of turbulent kinetic energy due to mean velocity gradients, G_b is the generation of turbulent kinetic energy because of buoyancy. Also, Y_M refers to the fluctuating dilation incompressible turbulence that contributes to the overall dissipation rate. In addition, S_ε and S_k are parameters defined by depending on the study performed. Moreover α_k and α_ε are indicated the turbulent Prandtl numbers for the turbulent kinetic energy and its dissipation. The eddy viscosity μ_t is calculated from equation 7 (Shih et al., 1995);

$$\mu_t=\rho C_\mu\frac{k^2}{\varepsilon} \quad (7)$$

The value of C_μ is calculated from equation 8 (Shih et al., 1995);

$$C_\mu=\frac{1}{A_0+A_S\frac{kU^*}{\varepsilon}} \quad (8)$$

$$U^*=\sqrt{S_{ij}S_{ij}+\widetilde{\Omega}_{ij}\widetilde{\Omega}_{ij}} \quad (9)$$

$$\widetilde{\Omega}_{ij} = \overline{\Omega}_{ij} - \varepsilon_{ijk}\omega_k - 2\varepsilon_{ijk}\omega_k \quad (10)$$

In the above equation, $\overline{\Omega}_{ij}$ is the average rate of rotation tensor which is observed in a rotating reference frame that has an angular velocity ω_k. The constants A_0 and A_s are as follows (Shih et al., 1995);

$$A_0 = 4.04\,,\ A_s = \sqrt{6}\cos\varphi \quad (11)$$

$$\varphi = \frac{1}{3}\cos^{-1}\left(\sqrt{6}\frac{S_{ij}S_{jk}S_{ki}}{\tilde{S}^3}\right),\quad \tilde{S} = \sqrt{S_{ij}S_{ij}}\,,\quad S_{ij} = \frac{1}{2}\left(\frac{\partial u_j}{\partial x_i} + \frac{\partial u_i}{\partial x_j}\right) \quad (12)$$

It is seen that the C_μ value is a function which is depended on the angular velocity, the rotational rates and the mean strain, its dissipation rate and the turbulent kinetic energy when considered the rotating system. The standard value of $C\mu = 0.09$ is obtained from the solution of equation 8 for an inertial sublayer in the equilibrium boundary layer (Shih et al., 1995):

$$C_1 = max\left(\frac{\psi}{5+\psi}, (0.43)\right) \quad (13)$$

$$\psi = S\left(\frac{k}{\varepsilon}\right) \quad (14)$$

$C_{1\varepsilon} = 1.44$ $C_2 = 1.9$ $\sigma_k = 1.0$ $\sigma_\varepsilon = 1.2$

G_b value for ideal gases;

$$G_b = -g_i\frac{\mu_t}{\rho Pr_t}\frac{\partial \rho}{\partial x_j} \quad (15)$$

$$C_{3\varepsilon} = \tanh\left|\frac{v}{u}\right| \quad (16)$$

k and ε are turbulent kinetic energy and dissipation rate, respectively.

$$\rho = \rho_0\left(1 - \beta(T - T_0)\right) \quad (17)$$

ϱ and β are reference density and coefficient of thermal expansion, respectively.

The discrete coordinate model (DO) is chosen to calculate the solar radiation coming into the system. The following equations are used in this model;

$$\nabla\cdot(I_\lambda(\vec{r},\vec{s})\,\vec{s}) + (\alpha_\lambda,\sigma_s)I_\lambda(\vec{r},\vec{s}) = \alpha_\lambda n^2 I_{b\lambda} + \frac{\sigma_s}{4\pi}\int_0^{4\pi} I_\lambda(\vec{r},\vec{s}')\,\Phi(\vec{r},\vec{s}')\,d\Omega' \quad (18)$$

α_λ, σ_s, n and λ are absorption coefficient, reflection coefficient, refractive index and wavelength, respectively. The total luminous intensity in the $\vec{s}$ direction is equal to the amount of spectral luminous intensity over the wavelength bands and is written as;

$$I(\vec{r},\vec{s}) = \sum_k I_\lambda(\vec{r},\vec{s})\,\Delta\lambda_k \quad (19)$$

In the SCPP, the Grashof number is expressed as;

$$Gr = \frac{g\beta}{\vartheta^2}\Delta T H^3 \quad (20)$$

$$\Delta T = T_{out} - T_{in} \quad (21)$$

ϑ and g represent kinematic viscosity and gravitational acceleration, respectively. The Richardson number is the ratio of the Grashof number to the square of the Reynolds number. If the Richardson number is over 10, forced convection; If it is below 0.1, natural convection can be neglected. Between 0.1 and 10, it represents a mixed convection flow in which both types of convection cannot be neglected (Shih et al., 1995).

$$Ri = \frac{Gr}{Re^2} \quad (22)$$

$$P = \frac{1}{2}B\dot{m}v^2 \quad (23)$$

$$\dot{m} = \rho A v \quad (24)$$

$\dot{m}$, ρ and A values are mass flow rate, density and cross-sectional area, respectively. P refers to the power obtained from the turbine. According to Betz's law, not all of the air coming into a turbine can be converted into kinetic energy. Up to 59.25% of the air coming into the turbine can be converted into kinetic energy. This value is called the Betz constant and is referred to B (Setia et al., 2021).

$$A = \pi R^2 \quad (25)$$

$$\eta = \frac{P}{IA} \quad (26)$$

A and η represent the surface area of the floor of the SCPP and the efficiency, respectively.

$$\eta_{col} = \frac{\dot{m}c_p\Delta T}{IA} \quad (27)$$

The commonly used expression of collector efficiency is expressed as η_{col}:

$$\eta_{chim} = \frac{gH}{c_p T_{out}} \quad (28)$$

For the efficiency of the chimney, the expression η_{chim} is used.

$$\eta_{SCPP} = \eta_{col}\eta_{chim} \quad (29)$$

$$\eta_{SCPP} = \frac{\dot{m}gH\Delta T}{IAT_{out}} \quad (30)$$

The expression η_{SCPP} is used for the efficiency of the SCPP.

4. RESULTS And DISCUSSIONS

Numerical analyzes were made for the SCPP with 4 different chimney heights. As a result of the analyzes made, the velocity gradients formed in the SCPP with a chimney height of 50 meters are seen in the Figure 5.

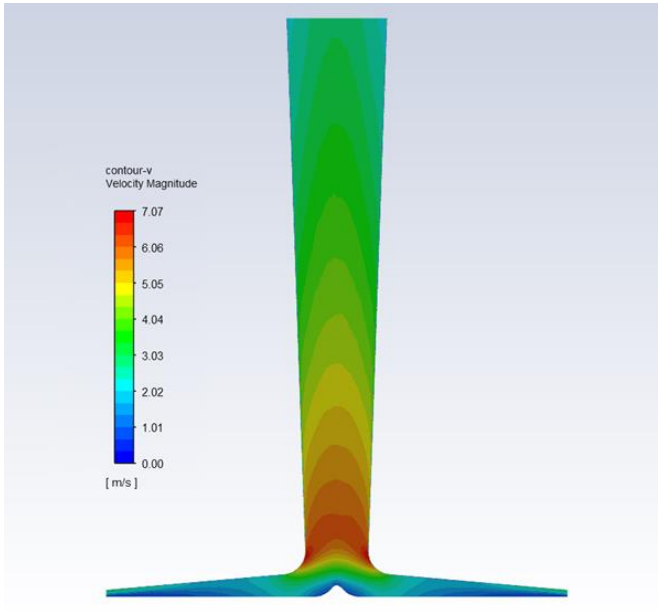

Figure 5. Velocity gradient

As seen in Figure 5, the velocity reaches its highest level in the narrow section of the chimney. Again, the pressure gradients formed in the SCPP with a chimney height of 50 meters are seen in the Figure 6.

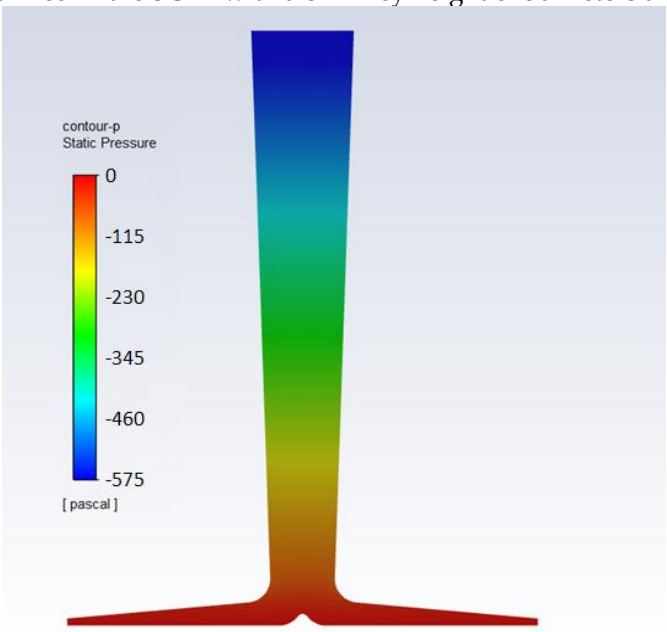

Figure 6. Pressure gradient

In many studies, since the inlet and outlet pressures are the same, pressure gradients are measured as atmosphere pressure on the ground and at the chimney outlet, and some negative pressure occurs in the narrow section of the chimney (Nasraoui et al., 2020). In this study, a pressure difference of 575 Pa occurs between the inlet and outlet points of the air. In Figure 6, it is seen that the pressure decreases regularly from the floor toward the chimney outlet. These pressure values read in Figure 6 are relative pressure values. The velocity vectors formed in the SCPP with a chimney height of 50 meters and in the narrow section of the chimney are comprehensively shown in the Figure 7.

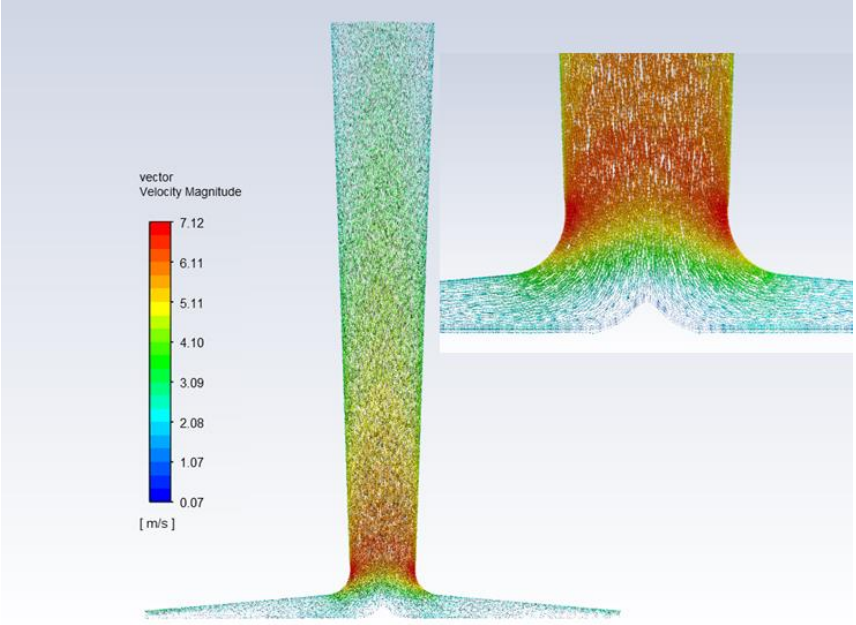

Figure 7. Velocity vectors

As the air enters the system at very low speeds at the collector inlet, its velocity increases rapidly as it moves towards the collector center. As the air enters the narrow section of the chimney, it changes direction and moves upwards. Since the air cannot change its direction suddenly at the junction of the collector and the chimney where this direction change is experienced, the vortex is occurred and energy losses are observed. In order to prevent these energy losses while designing, a curve with a radius of 2 m was formed on the chimney and collector connection area. In this way, all velocity vectors are aligned upwards in the narrow section of the chimney Since the SCPP is expanded an angle of 2 degrees towards the chimney outlet, the air velocity decreases as one moves towards the solar chimney outlet. The temperature distribution formed in the cross-section of the SCPP which has a chimney height of 50 meters is shown in the Figure 8.

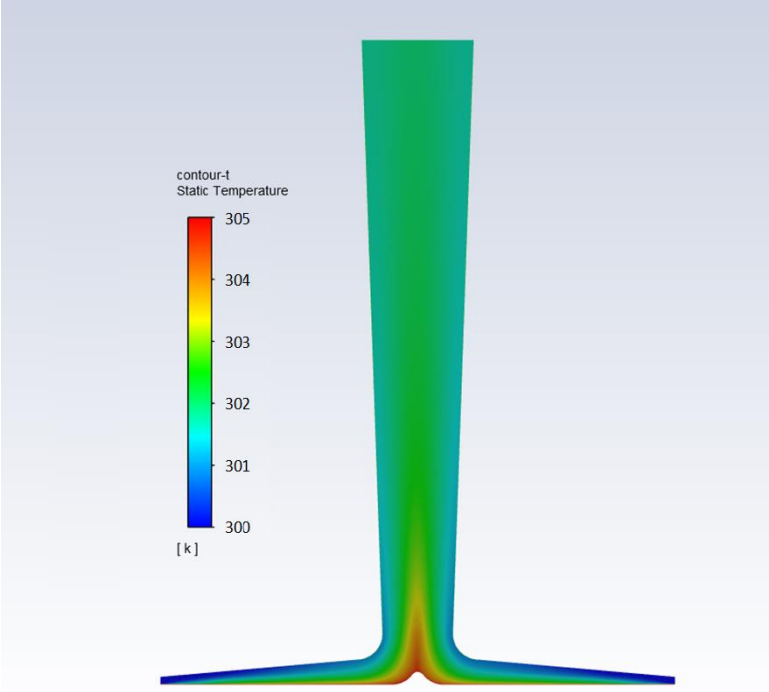

Figure 8. Temperature gradient

As solar radiation is absorbed by the ground, an increase in temperature is observed on the ground. Due to the increase in the temperature difference between the air and the ground, the heat transfer rate is increased and the air temperature is started to increase in the regions near the ground.

As the air is transmitted into the center of the collector, its temperature continues to increase until it reaches the chimney inlet. In the region below the chimney inlet, this temperature reaches the highest value. Then, as the air rises from the chimney, the temperature is distributed homogeneously and the average temperature remains constant throughout the adiabatic chimney. The numerical analyzes are performed for 4 different SCPPs which have 50, 100, 150 and 200 meters height. As a result of the analyzes made, the velocity, mass flow rate and chimney outlet temperature values formed in the narrow section of the chimney are shown in the Figure 9.

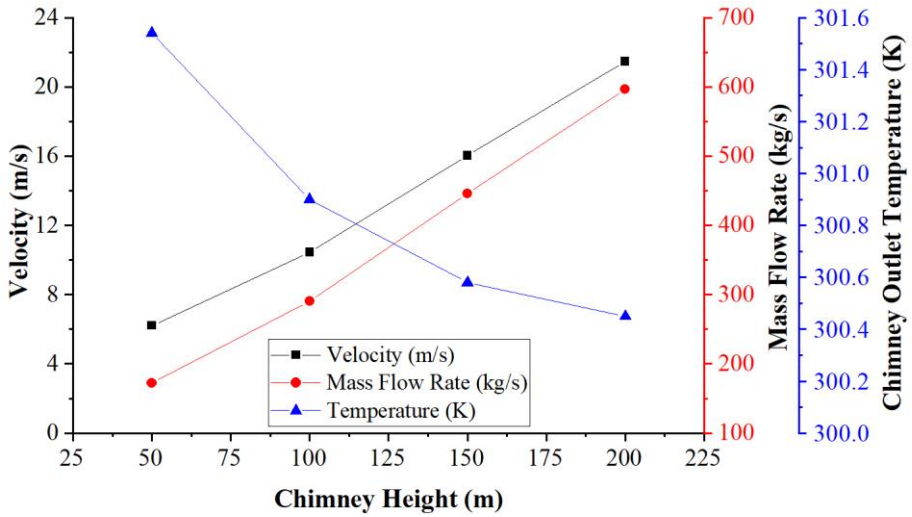

Figure 9. The velocity, mass flow rate and chimney outlet temperature values formed in the narrow section of the chimney

The narrow section of the chimney is where the speed is highest throughout the entire system and therefore the turbine is placed in this region. Basically, there are two main parameters that increase the speed value. While the first of these is the collector diameter, the second is the height of the chimney. Firstly, as the collector diameter increases, the total amount of radiation entering the system also increases. Also, the high amount of radiation is increased the floor temperature and therefore the heat transfer rate is heightened. In this way, after the air temperature increases, the heated air is swiftly raised. In addition, the density of the heated air on the ground decreases and it is subjected to a force along the chimney due to the density difference. Secondly, as the height of the chimney increases, it is observed that it is more exposed to this force and the velocity of the working fluid increases. The lowest and highest velocity values in the narrow section of the chimney were calculated as 6.22 m/s and 21.46 m/s for 50 and 200 m chimney heights, respectively.

As soon as the air enters the system, the velocity of the working fluid is varied depending on the cross-sectional area, but the mass flow rate is constant. The measured mass flow rate values at the collector inlet, chimney outlet and narrow section of the chimney are the same. As the height of the chimney increases, negligible changes are observed in the density value, on the other hand, although the cross-sectional area is not changed, and the velocity value changes dramatically. Therefore, considering equation 24, it is seen that the mass flow rate and velocity value are increased in direct proportion to each other. In Figure 9, it is seen that the mass flow rate values formed in the narrow section of the chimney are directly proportional to the height of the chimney. When evaluated the mass flow rate results in the graph, while the lowest mass flow rate in the narrow section of the chimney was calculated as 172.45 kg/s at the 50 m chimney height, the highest mass flow rate is found as 596.22 kg/s at 200 m at chimney height.

As the height of the chimney increases, it is clearly seen that the speed and flow values are increased with the effect of the pressure difference, but the temperature values decrease. The reason for this is that the amount of air in contact with the ground increases thanks to the rising air velocity, and more air mass shares the heat transferred from the ground. For this reason, the amount of increase in the temperature of the air decreases as the height of the chimney increases. The lowest and highest temperature values at the chimney outlet are calculated as 300.45-301.54 K for 200 and 50 m chimney heights, respectively. The power and efficiency values calculated depending on the changing chimney heights are shown in the Figure 10.

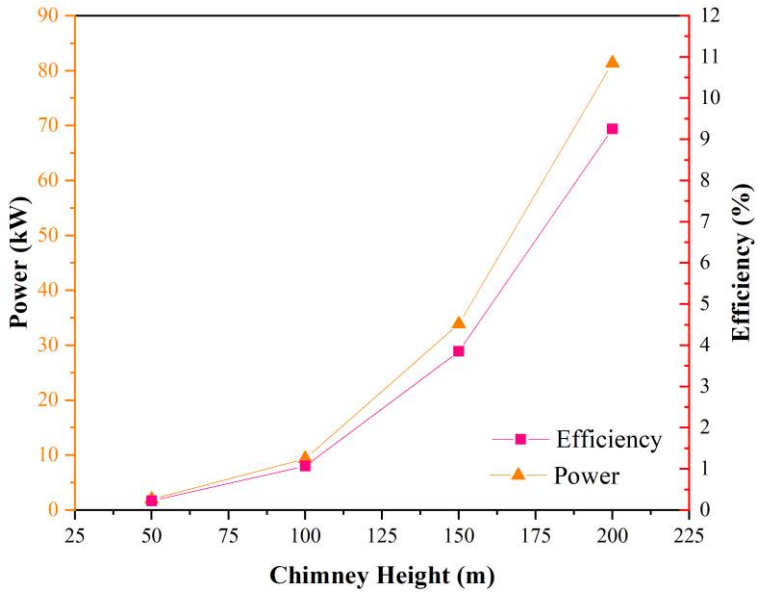

Figure 10. Power and efficiency values

While calculating power and efficiency values of the SCPP, equation 23 and equation 26 are used, respectively. Starting from equation 23, it can be said that power is proportional to the cube of the velocity when the changes in density are ignored. As the height of the chimney increases, the velocity value is increased and therefore the power value of the SCPP obtained is also increased in direct proportion to the cube of the velocity. The efficiency value of the SCPP is the ratio of the obtained power to the total solar radiation entering the system. Since the total solar radiation is not changed as the height of the chimney increases, the efficiency value of the SCPP is changed directly proportional to the power. For this reason, the efficiency value of the SCPP is increased in direct proportion to the cube of the speed as the height of the chimney increases, just like the power value. Among the designs, the lowest and highest power and efficiency values were calculated as 1.97 kW, 81.38 kW and 0.22%, 9.25% for 50 and 200 m chimney heights, respectively. In the Table 3, some efficiency values obtained in this study are compared with the efficiency values obtained from other studies in the literature.

Table 3. Efficiency values

Study	H (m)	η (%)	η_{col} (%)	η_{chim} (%)	η_{SCPP} (%)
This study	50	0.22	30.3	0.16	0.049
	100	1.07	29.9	0.32	0.097
	150	3.85	29.5	0.49	0.144
	200	9.25	30.8	0.65	0.200
Sivaram et al., 2020	0.45	-	26.4	0.45	0.0012
Das and Chandramohan, 2019	6	-	60.5	0.025	0.0018
Al-Kayiem et al., 2019	6.65	-	64.0	-	-
Xu and Zhou, 2018	194.6	-	29.4	-	-
Zuo et al., 2020	194.6	-	13.5	-	-

In the Table 3, it is seen that when a few studies focusing on the SCPP is evaluated, the efficiency values of the SCPP are calculated by using different equations. In some studies, giving the collector efficiency is sufficient, while in others, this value is multiplied by the chimney efficiency to obtain the solar chimney efficiency. When the obtained values are compared to each other, it has been determined that the collector efficiency is an independent value from the chimney height, but the chimney efficiency is directly proportional to the chimney height. For this reason, as the height of the chimney is increased, although the collector efficiency remained constant, the efficiency of the chimney and solar chimney increased.

5. CONCLUSION

The SCPP generates power thanks to the rays of the sun, which is one of the renewable energy sources. The amount of the generated power and efficiency of the SCPP is directly related to the geometric design of the system. In this study, the SCPP was designed for 4 different chimney heights and the design was analyzed by means of a numerical analysis program. As a result of the analyzes:

- It was determined that as the height of the chimney increases, the velocity, mass flow rate, power and efficiency values increase, but the temperature difference decreases.
- Another efficiency value was defined because efficiency expressions stated in other studies were insufficient since the main reason is that the collector efficiency and solar chimney efficiency expressions are not dependent on the power to be obtained from the system.

- In order to obtain maximum power from the system, a turbine was placed in the narrow section of the chimney.
- The highest velocity, mass flow rate, power and efficiency values obtained from the SCPP are found to be 21.46 m/s, 596.22 kg/s, 81.38 kW and 9.25%, respectively.

NOMENCLATURE

CFD	= computational fluid dynamics
SCPP	= solar chimney power plant
B	= Betz constant

SYMBOLS

c_p	= specific heat (kJ/kgK)
$\dot{m}$	= mass flow rate kg/s)
P	= pressure (Pa) and power (W)
T	= temperature (K)
T_0	= ambient temperature (K)
v	= velocity (m/s)
ρ	= intensity (kg/m^3)
η	= efficiency (%)
k	= kinetic energy
ε	= rate of dissipation of kinetic energy
I	= solar radiation (W/m^2)

SUBSCRIPTS

in	= inlet
out	= outlet
col	= collector
$chim$	= chimney

REFERENCES

Al-Kayiem, H. H., Aurybi, M. A., Gilani, S. I., Ismaeel, A. A., & Mohammad, S. T. (2019). Performance evaluation of hybrid solar chimney for uninterrupted power generation. Energy, 166, 490-505.

Cable, M. (2009). An evaluation of turbulence models for the numerical study of forced and natural convective flow in Atria (Doctoral dissertation, Queen's University), 25-38.

Das, P., & Chandramohan, V. P. (2019). Computational study on the effect of collector cover inclination angle, absorber plate diameter and chimney height on flow and performance parameters of solar updraft tower (SUT) plant. Energy, 172, 366-379.

Das, P., & Chandramohan, V. P. (2020). 3D numerical study on estimating flow and performance parameters of solar updraft tower (SUT) plant: Impact of divergent angle of chimney, ambient temperature, solar flux and turbine efficiency. Journal of Cleaner Production, 256, 120353.

Haaf, W., Friedrich, K., Mayr, G., & Schlaich, J. (1983). Solar chimneys part I: principle and construction of the pilot plant in Manzanares. International Journal of Solar Energy, 2(1), 3-20.

Karami, S., Roghabadi, F. A., Maleki, M., Ahmadi, V., & Sadrameli, S. M. (2021). Materials and structures engineering of sun-light absorbers for efficient direct solar steam generation. Solar Energy, 225, 747-772.

Kebabsa, H., Lounici, M. S., Lebbi, M., & Daimallah, A. (2020). Thermo-hydrodynamic behavior of an innovative solar chimney. Renewable Energy, 145, 2074-2090.

Koç, A., Yağlı, H., Bilgic, H. H., Koç, Y., & Özdemir, A. (2020). Performance analysis of a novel organic fluid filled regenerative heat exchanger used heat recovery ventilation (OHeX-HRV) system. Sustainable Energy Technologies and Assessments, 41, 100787.

Mert, İ., Bilgic, H. H., Yağlı, H., & Koç, Y. (2020). Deep neural network approach to estimation of power production for an organic Rankine cycle system. Journal of the Brazilian Society of Mechanical Sciences and Engineering, 42(12), 1-16.

Nasraoui, H., Driss, Z., & Kchaou, H. (2020). Novel collector design for enhancing the performance of solar chimney power plant. Renewable Energy, 145, 1658-1671.

Nassar, Y. F., Abdunnabi, M. J., Sbeta, M. N., Hafez, A. A., Amer, K. A., Ahmed, A. Y., & Belgasim, B. (2021). Dynamic analysis and sizing optimization of a pumped hydroelectric storage-integrated hybrid PV/Wind system: A case study. Energy Conversion and Management, 229, 113744.

Roy, D., & Samanta, S. (2021). Development and multiobjective optimization of a novel trigeneration system based on biomass energy. Energy Conversion and Management, 240, 114248.

Setia, G. A., Zaen, Z. Z., Haz, F., Iskandar, H. R., Winanti, N., & Hidayat, M. R. (2021, October). Optimization of the Hybrid Power Plant Design (PV-Wind) for Residential Load. In 2021 3rd International Conference on High Voltage Engineering and Power Systems (ICHVEPS) (pp. 227-231). IEEE.

Shih, T. H., Liou, W. W., Shabbir, A., Yang, Z., & Zhu, J. (1995). A New Eddy-Viscosity Model for High Reynolds Number Turbulent Flows-Model Development and Validation.-Computers Fluids. 24 (3). 227-238.

Singh, A. P., Kumar, A., & Singh, O. P. (2020). Performance enhancement strategies of a hybrid solar chimney power plant integrated with photovoltaic panel. Energy Conversion and Management, 218, 113020.

Sivaram, P. M., Mande, A. B., Premalatha, M., & Arunagiri, A. (2020). Investigation on a building-integrated passive solar energy technology for air ventilation, clean water and power. Energy Conversion and Management, 211, 112739.

Tan, J. D., Chang, C. C. W., Bhuiyan, M. A. S., Nisa'Minhad, K., & Ali, K. (2022). Advancements of wind energy conversion systems for low-wind urban environments: A review. Energy Reports, 8, 3406-3414.

Xu, Y., & Zhou, X. (2018). Performance of divergent-chimney solar power plants. Solar Energy, 170, 379-387.

Zuo, L., Liu, Z., Ding, L., Qu, N., Dai, P., Xu, B., & Yuan, Y. (2020). Performance analysis of a wind supercharging solar chimney power plant combined with thermal plant for power and freshwater generation. Energy Conversion and Management, 204, 112282.